NCT Magnet Enables High-Temperature Ferromagnetism and Giant Topological Transport

Yuxuan Zhou[1†], Ke Yang[2,1†], Yaozhenghang Ma[1], Feng-Ren Fan[3,1], and Hua Wu[1*]

1. Laboratory for Computational Physical Sciences (MOE), State Key Laboratory of Surface Physics, and Department of Physics, Fudan University

2. College of Science, University of Shanghai for Science and Technology

3. Institute for Quantum Science, School of Physical Science and Technology, Soochow University

Introduction

The design of high-performance van der Waals magnets is limited by the trade-off between robust 3*d* magnetism and strong 5*p* spin-orbit coupling. Here, we show that $MnSiTe_3$ overcomes this limitation through a **negative charge-transfer** mechanism, where itinerant Te 5*p* ligand holes mediate strong ferromagnetic exchange and enhance magnetic anisotropy. This mechanism also couples magnetism with topological electronic states, enabling robust anomalous Hall responses and suggesting a route toward room-temperature spintronics in 3*d*-5*p* vdW magnets.

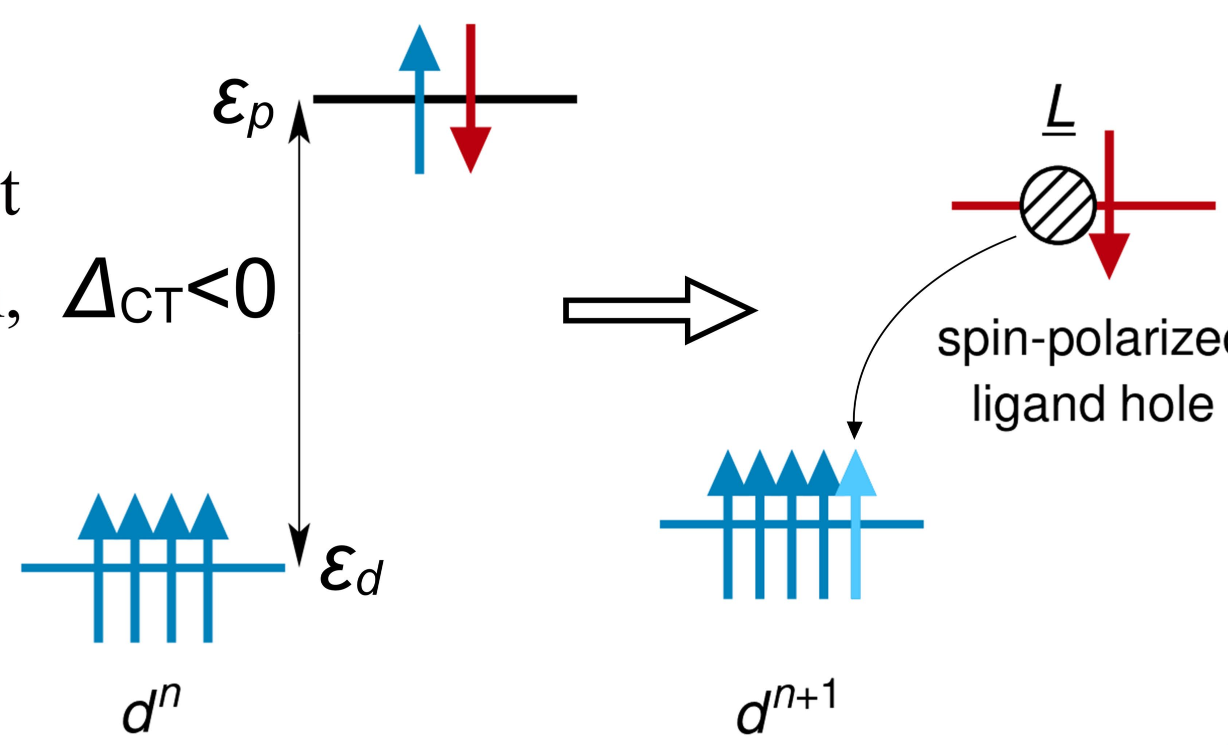

Charge State

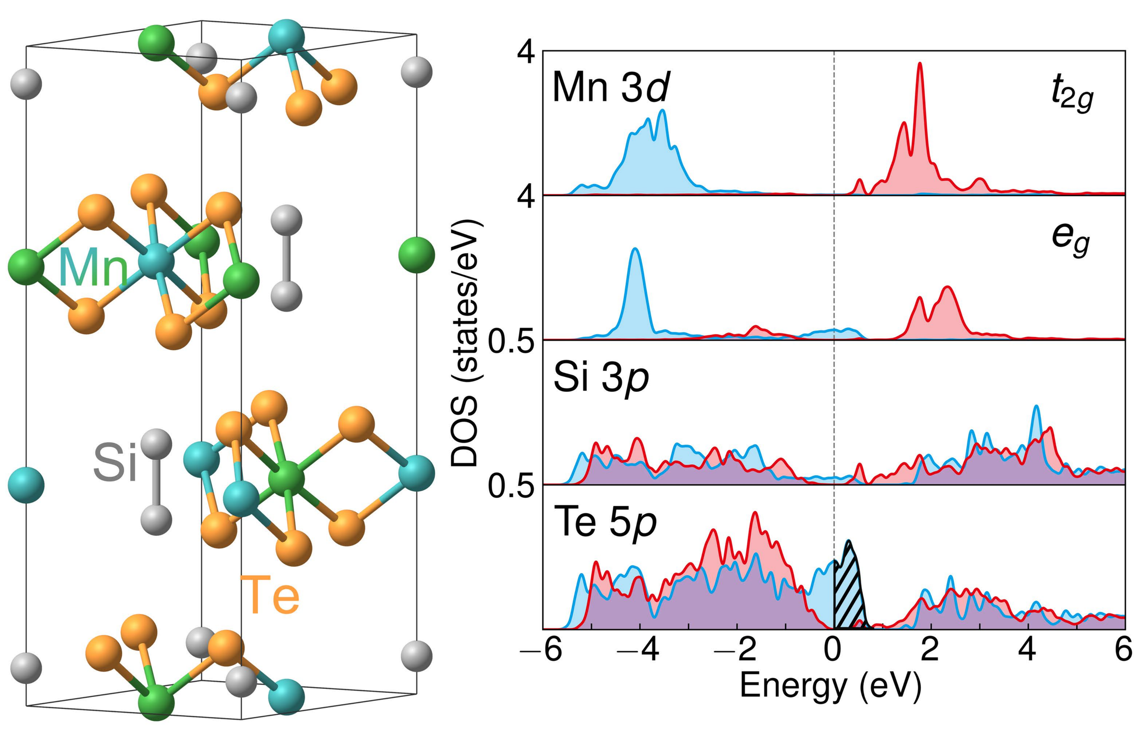

Si-Si dimer ~ Si^{3+}

Formal (d^n):
Mn^{3+} Te^{2-}
$3d^4$ — $5p^6$ ✗

NCT ($d^{n+1}\underline{L}$):
Mn^{2+} $S=5/2$ ~ $3d^5$ ✓
1 hole/f.u. for Te ~ $\underline{L}$

***p-d* exchange: FM Metallic**

Intra- and Inter- Layer Coupling

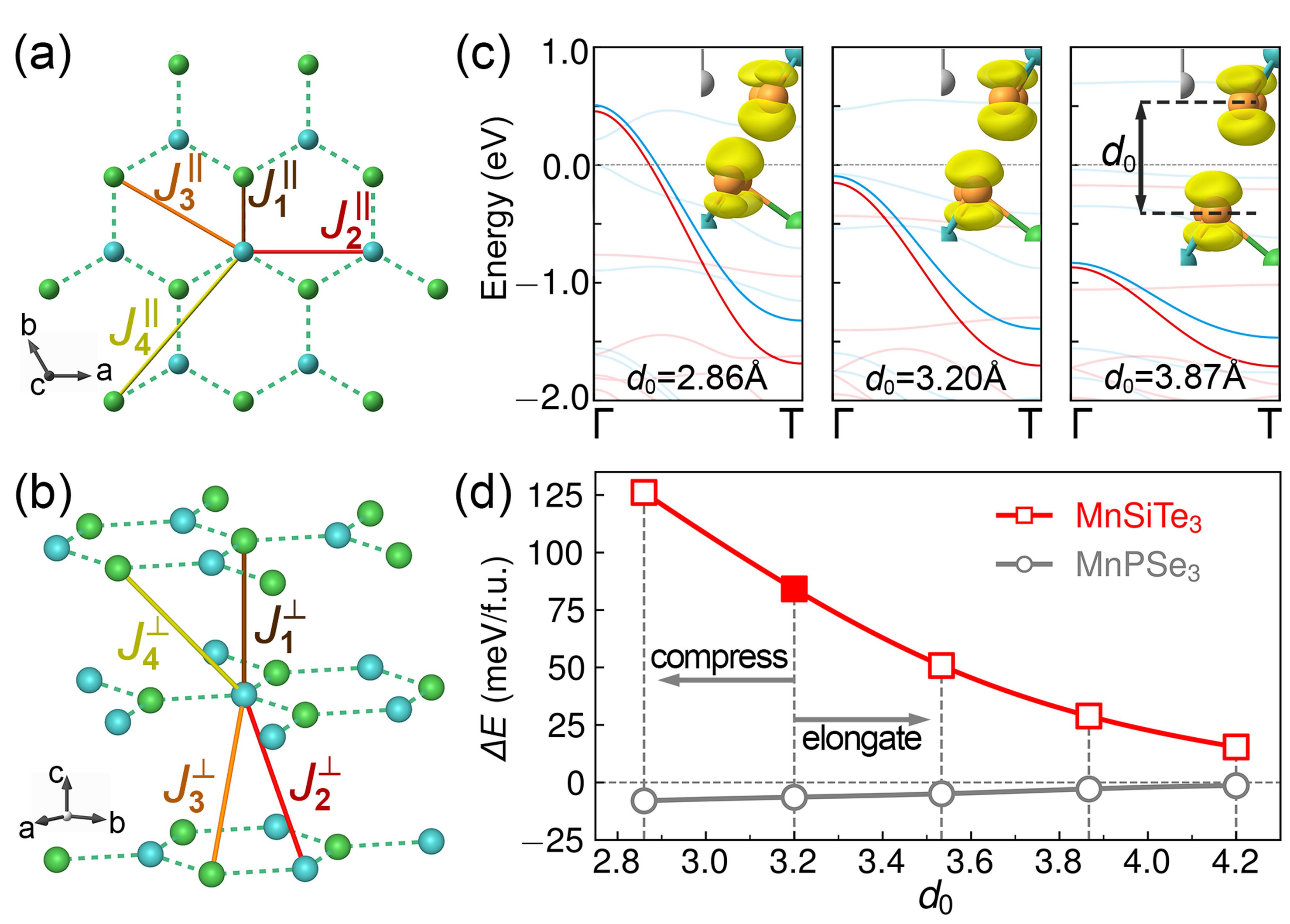

Large intraplane: itinerant 5*p* hole

Large interplane: fat p_z orbital along *z*-direction

(a) Intralayer and (b) interlayer magnetic interactions. (c-d) Detailed interlayer interactions for varying d_0. (c) Band structure near E_F, blue (red) represents spin-up (down) component. Insets show the corresponding wavefunction for highlighted band. (d) Energy differences between the interlayer FM and AF states for bulk $MnSiTe_3$ and $MnPSe_3$.

Te-dominated MAE

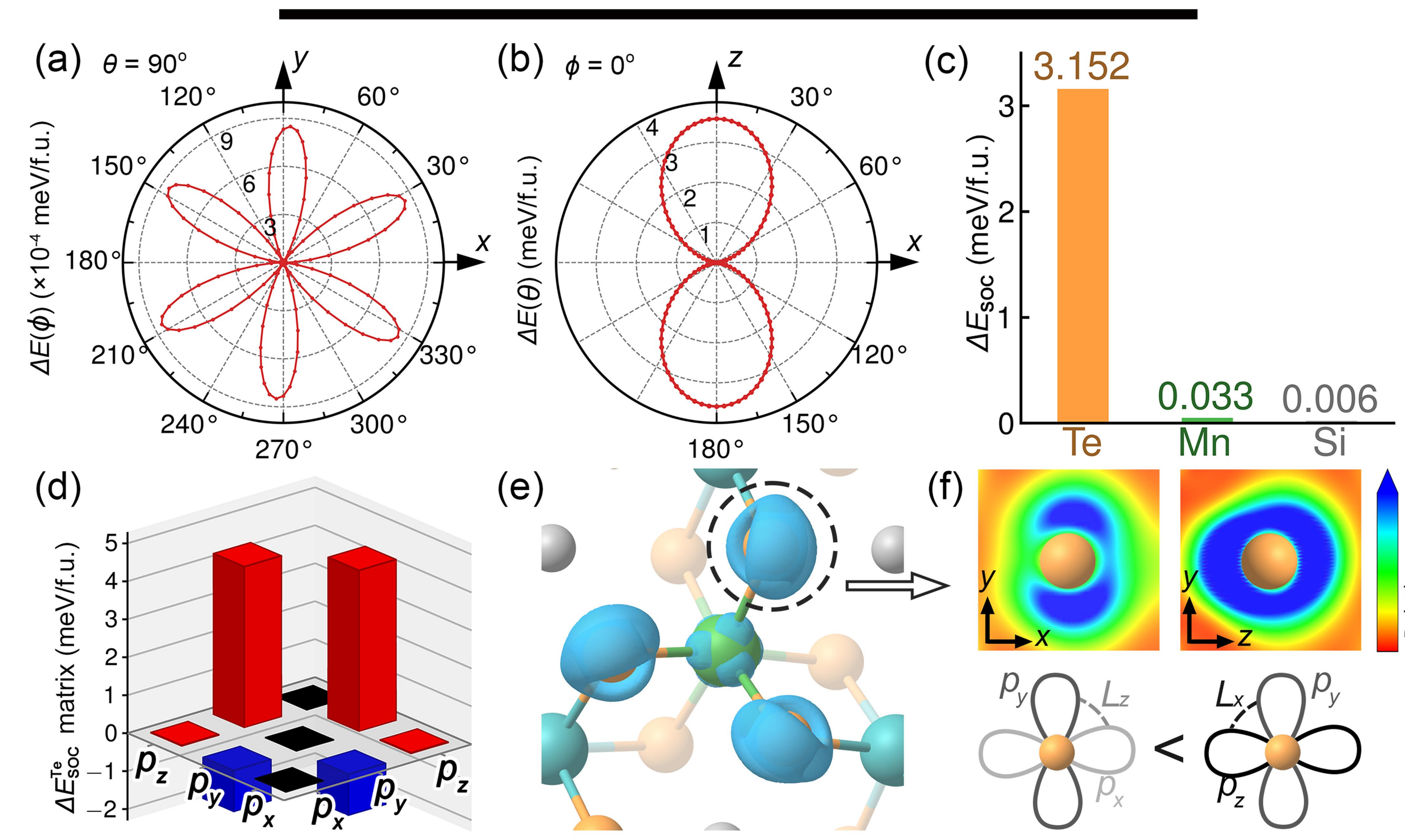

Te 5*p* hole: ligand *Single-ion* Anisotropy

(a, b) Calculated MAE as a function of magnetization direction for in-plane rotation at $\theta = 90°$ and out-of-plane rotation at $\phi = 0°$, respectively. (c) Element-resolved SOC contribution to the MAE, showing the dominant contribution from Te. (d) Orbital- resolved MAE matrix for the Te 5*p* orbitals when ***M*** is along *x*-axis. (e) Partial charge density of the near-Fermi-level states integrated over $E_F \pm 0.1$ eV(f) Slices of (e) in the xOy and yOz planes. The lower panels illustrate the corresponding couplings between Te 5*p* orbitals.

Giant anolalous Hall effect

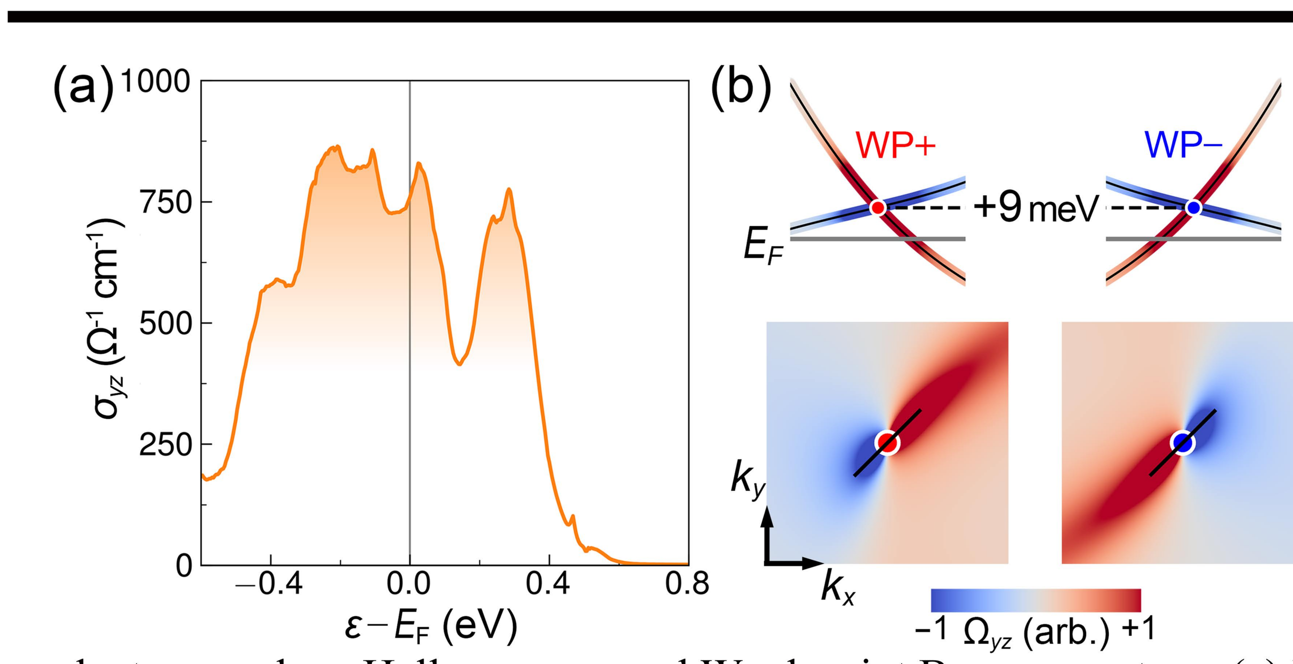

Energy-dependent anomalous Hall response and Weyl-point Berry curvature: (a) Energy dependence of the *yz* component of AHC. (b) Nearest Weyl point pair (WP±) around E_F, located just 9 meV above E_F. Local band dispersion is colored by Ω_{yz}. Below is the local k_z-integrated map on the k_x - k_y plane of Ω_{yz}.

Summary

3*d*-5*p* NCT spin-polorized ligand hole ⇒ itinerant FM half-Metallic ⇒ High T_C ~ 464K

3*d*-5*p* NCT spin-polorized ligand hole ⇒ heavy 5p orbital large SOC ⇒ ligand dominated MAE (in-plane 3.6 meV/f.u.) ⇒ High T_C ~ 464K

heavy 5p orbital large SOC ⇒ Topological Response (σ^A ~ 760 $\Omega^{-1}cm^{-1}$)